Advancements in Human Breast Organoid Culture: Modeling Complex Tissue Structures and Developmental Insights

Gat Rauner[1*], Nicole C. Traugh[1,2], Colin J. Trepicchio[1,2], Meadow E. Parrish[1,2], Kenan Mushayandebvu[3], Charlotte Kuperwasser[1, 2, 4*]

Affiliations:

[1] Department of Developmental, Molecular & Chemical Biology, Tufts University School of Medicine, Boston, MA 02111, USA

[2] Program of Genetics, Molecular & Cellular Biology, Tufts Graduate School of Biomedical Sciences, Boston, MA 02111, USA

[3]Department of Biology, Tufts University School of Arts and Sciences, Medford, MA 02155, USA

[4] Laboratory for the Convergence of Biomedical, Physical, and Engineering Sciences, Tufts University School of Medicine, Boston, MA 02111, USA

These authors contributed equally: Gat Rauner, Nicole C. Traugh, Colin J. Trepicchio.

***Correspondence should be addressed to:**
Charlotte Kuperwasser (charlotte.kuperwasser@tufts.edu);
Gat Rauner (gat.rauner@tufts.edu).

Abstract

Organoids have been widely used for studying tissue growth and modeling diseases, but achieving physiologically relevant architecture, size, and function has remained a challenge. Here, we develop a next-generation organotypic culture method that enables the formation of a highly patterned, complex, branched tissue that is spatially organized to accurately recapitulate the morphology, scale, cellular, transcriptional, and tissue-level heterogeneity of human breast tissue. Hormone responsiveness of organoids is also a feature allowing for examination of androgen therapy or post-menopausal changes to breast tissue development and regeneration. Live imaging allows for studying stem cell dynamics during organoid formation and is adaptable to a high throughput setting. Real-time imaging of organoid formation reveals activation of latent epithelial organogenesis programs and inductive cellular dynamics that drive formation of a miniature breast tissue along with its mesenchyme akin to tissue stroma. By advancing human breast organoid technology, this model can elucidate cell- and tissue-level consequences to hormonal changes and therapy. In addition, this method can lead to new insights into the cellular, molecular, and tissue-level processes involved in organogenesis and regeneration, as well as disease.

Main

Organogenesis, including tissue morphogenesis, is essential in the development and maintenance of multicellular organisms. This process involves the coordination of cell behavior and organization, allowing for the formation of functional tissues and organs. Understanding how tissues develop and form is crucial for understanding how they work and how they can be repaired or regenerated in the case of disease or injury. In addition, defects in organogenesis can lead to developmental disorders and birth defects, and insights into cellular and molecular mechanisms that are disrupted can potentially lead to new treatments or preventative measures. Finally, understanding how cells communicate and work together to form complex structures and systems has implications for a wide range of fields beyond developmental biology, including tissue engineering and regenerative medicine.

Organoids are miniaturized and simplified versions of organs produced in vitro in three dimensions that show realistic micro-anatomy. They are derived from stem cells and can replicate some of the organ's structure and function. Human breast organoids have emerged as a promising tool for studying developmental processes and breast cancer [1-3]. However, these organoids are mostly spheroid and rudimentary, and thus are unable to establish physiologically relevant complex patterning, hormonal sensitivity, scale, or relevant architectural complexity. Most traditional breast organoid models rely on an extracellular matrix scaffold composed entirely from Matrigel or Type I Collagen, which only provides a supportive microenvironment for cells to promote self-assembly of simple and rudimentary structures [4-9]. Thus, traditional breast organoid models have limited value in studying tissue morphogenesis and disease, including cancer, as they lack many of the key features of the organ.

Development of improved biomimetic ECM scaffolds is an active area of research, with the goal of providing more accurate and reproducible models of in vivo tissue microenvironments. Recently, collagen-based hydrogels containing components that are part of the human breast ECM: fibronectin, laminin, and hyaluronic acid have been reported [10]. Here we describe a method of creating next generation organotypic cultures using this newly described biomimetic ECM scaffold. From a single adult human breast stem cell, a miniaturized human breast is generated, comprised of several terminal ductal-lobular units (TDLUs). We combine this method with high-throughput, high-speed confocal live-imaging microscopy to study organoid formation, frequency, and regenerative capacity. Further by real-time imaging, we find that organoid formation goes through stages of directed epithelial organogenesis including the de-novo creation of its own stroma rather than spontaneous self-assembly. We also evaluate organoid formation from cells obtained from post-menopausal women and female-to-male (F-M) transition patient breast tissue to study the effects of hormonal changes in vivo on organogenesis and regeneration capacity ex vivo. Together, these findings describe a robust method for generating, studying, and tracking patient-derived biomimetic breast tissue, that can be used for clinical and basic biology studies.

Results

Regeneration, architecture, and patterning of patient derived organoids from single cells

Organoids were generated from primary single cells isolated from normal, disease free fresh reduction mammoplasties (n=12; age 18-40, BMI < 30, Fig. 1a). Patient-to-patient variability in organoid generation capacity was evaluated by thoroughly analyzing whole-gel confocal images taken at 5-6 focal planes (Z) and quantifying the number of organoid structures formed. When seeded as single cells all but one patient sample yielded organoids over a 19-day period. Three types of structurally distinct organoids develop in these cultures. (1) The most common type are ductal-lobular structures that consist of branched elongated ducts that terminate with alveoli (60.48% ± 7.96% mean ± STD). (2) Ductal structures with no alveoli are the second most common type (31.17 ± 11.77% mean ± STD), followed by (3) acinar structures with no visible ducts (8.35 ± 5.06% mean ± STD) (Fig. 1b, c). Significant variability is observed in average organoid formation frequency between patients, (Fig. 1d), and no correlation was found between regeneration capacity and patient age (R^2=0.007) or BMI (R^2=0.003). Across the 12 patient samples, the median number of structures formed per 100 seeded cells was 1.775, with a 95% CI between 0.45 and 4.10 (Fig. 1e).

Secondary organoid formation was performed to evaluate the regenerative capacity of stem/progenitor cells within formed structures. Primary organoids established from five patient samples were dissociated and single cells were re-seeded into a second set of hydrogels (n=4 per sample). The number of secondary organoids that formed by day 17 was quantified. In all five patient samples, we observed a reduction in secondary organoid formation compared to primary organoid formation (Fig. 1f) suggesting a reduction in either stem cell number or regenerative

capacity of stem cells. The median number of secondary structures formed per 100 seeded cells was 1.067, with a 95% CI between 0.23 and 1.37 (Fig. 1g). Interestingly, there was greater patient-to-patient variability in primary organoid formation compared to secondary organoid formation, suggesting that once organoids form, they maintain a relatively consistent pool of regenerative cells within them.

Organoids show physiologically accurate architecture, size, and cell patterning of human breast tissue. TDLUs with ducts terminating in lobules was recapitulated in organoids with luminal cells expressing E-cadherin and basal cells encapsulating them and expressing CK14 (Fig. 1h). Side-by-side comparison of breast tissue sections with organoids show a similar expression pattern of the luminal marker E-Cadherin and the basal markers CK14 (Fig. 1i). Together these results show that next-generation organoid formation undergoes a series of well-coordinated events that result in the formation of a multi-layered biomimetic breast tissue that accurately resembles complex and heterogenous breast tissue.

Comparative Transcriptional Analysis of Tissue and Organoid Cell Populations

To ascertain if next-generation organoids mirror human breast tissue, we performed a side-by-side analysis using single-cell RNA sequencing (scRNA-seq) on cells from organoids[11] and directly from normal human breast tissue[12]. The integrated data revealed six cell populations that were shared between human breast tissue and organoids (Fig. 2a). There were three populations of luminal cells, one population of basal cells, and interestingly, two mesenchymal populations (Fig. 2a). The majority of the cells exhibited transcriptional characteristics of epithelial cells, while a prominent population of cells defined by stromal genes was observed. Not surprisingly, human breast tissue displayed additional clusters not found in organoids,

reflecting the greater cellular diversity and intricacy of in vivo tissue. The clusters unique to human breast tissue represented three immune cell populations - T cells, dendritic cells, and B cells, as well as vascular cell populations.

The luminal and basal epithelial cells in organoids showed clustering patterns similar to those in their in-vivo counterparts. This indicates that the cells within the organoids possess transcriptional profiles and traits akin to cells in natural tissues (Fig. 2a). Three sub populations of luminal cells were identified due to their differing gene expression profiles: Luminal 1, Luminal 2, and Luminal 3. All three populations expressed the classic luminal epithelial markers KRT8, KRT18 and KRT19, as well as CD24 (Fig. 2b-e). However, Luminal 1 cells expressed the hormone receptors genes ESR1 and PGR (Fig. 2f,g), while Luminal 2 and Luminal 3 cells lacked these genes. Luminal 3 cells expressed ELF5, SFRP1, and KIT linking this population more closely with mature luminal cells (Fig. 2h-j). Luminal 2 however, expressed genes associated with both basal and luminal markers, which could be a luminal-basal population (Fig. 2b-e, h-m). Basal cells on the other hand expressed the classic basal epithelial markers KRT5, KRT14, and KRT17 (Fig. 2k-m). Notably, we observed a non-epithelial cell population within the organoid cultures, that corresponded to a population of stromal fibroblasts found in-vivo (Fig 2a). This mesenchymal population expressed the stromal markers PDGFRB, COL1A2, COL6A3, THY1, and ZEB1 (Fig 2n-r).

These results emphasize our organoid model's proficiency in mirroring critical features of human breast tissue. Next-generation organoids recreate a significant portion of the cellular diversity of actual breast tissue including the varied functionalities of luminal cells as well as mesenchymal cells. The scRNA-seq results highlight our organoid's ability to mimic distinct cell populations observed in natural breast tissue, with the luminal and basal cells particularly

resembling their in-vivo counterparts. Together, this affirms our organoid's capacity as a biologically relevant model for studying breast tissue biology and associated disorders.

High-throughput, long-term live confocal imaging of organoid formation

We modified the organotypic culture methodology to enable high throughput and high-speed live-imaging confocal microscopy (Fig. 4a). We scaled down the hydrogel volume from 200 to 20 μl gels to accommodate a 96-well format. Patient-derived primary breast epithelial cells were labeled with a cell tracking dye (Cytopainter Green) to distinguish them from cell debris on the day of seeding. This step was important to improve the visualization and ensure the tracking of live primary cells, which are difficult to distinguish morphologically at this early stage. Labeled cells were seeded at a density of 100 cells per hydrogel and cultured for 2.5-3 weeks. Cultures were kept in a stage-top incubator that maintained controlled temperature, CO_2 levels, and humidity, all within an enclosed dark chamber attached to a confocal microscope. We live tracked 111 locations on the plate, capturing 9 Z planes spanning 160 μm every 30-45 minutes over the 18-21 day period. This methodology allowed for unprecedented visual documentation of organoid formation in real time.

We observed that organoid formation occurs in 4 distinct phases: Induction, Patterning, Morphogenesis & Maturation spanning approximately 18 days. The full process of organoid development, encompassing all four phases, is illustrated in Fig. 3b, c and Supplementary Videos 1-7. Inductive interactions, especially between the epithelium and the ECM is crucial for organ initiation [13,14] and can be seen in real-time in this model. We observed organoid induction as a distinct preliminary stage, taking place from days 0 to 8. During the Induction Phase, cells exhibit

minimal movement and largely stay stationary, with the initiation of cell proliferation. We observed two distinct induction types: Type I, the predominant type that starts with isolated, dispersed, spindle-shaped cells (Fig. 3b and Supplementary Videos 1-4, 6) and Type II, that begins with close-packed cells in a spheroid from which individual cells emerge. The ejection of cells from the spheroid colony initiates the next phase - Patterning. (Fig. 3d and Supplementary Video 5). Over the next ~10 days, colonies begin to pattern into rudimentary branches in dynamic process of cell trafficking where individual cells migrate back and forth along the axis of the extending branch. In contrast to the classic branching process that proceeds through steady invasion of a fully formed bud spearheaded by leader cells[15,16], we observed that organoid patterning proceeds through dispersed motile cells establishing a "blueprint" of the organoid branching pattern. This blueprint is subsequently populated with the cells that structurally form these branches in the succeeding Morphogenesis phase. Morphogenesis is characterized by formation of three-dimensional structures, such as tubes, buds, and cavities. While the organoid is undergoing morphogenesis, highly motile cells continue to rapidly proliferate and surround the morphing organoid. These cells appear to form a mesenchyme that supports the organoid and facilitates its differentiation and maturation.

During embryogenesis, the early ectoderm is the precursor to both the stromal and epithelial components of the breast, and expression of epithelial markers such as CK14 and E-Cadherin begins during the process of epithelialization [17-20]. Notably, we found that during induction, neither CK14 nor E-cadherin are expressed in the single cells that have not yet formed an organoid (Fig. 3e). However, by day 10 day, the epithelial marker CK14 is expressed when basal epithelial cells appear, consistent with commitment to the epithelial lineage. Interestingly, highly motile cells that give rise to a mesenchyme appear to originate from the same cells that

generate the organoid (Supplementary Video 6). E-cadherin, which is crucial for epithelial cell-cell adhesion is expressed when luminal cells appear within the inner layer of the thickening branches by day 15. This localization of E-Cadherin during morphogenesis is most predominant at locations within structures that will become the alveoli (Fig. 3e).

The final stage of organoid formation is the Maturation Phase that occurs around day 16-19. During this stage, the tissue adopts the typical structure of a TDLU, that consists of round alveoli grouped together and connected by ducts set within a mesenchymal matrix. The mesenchyme induces contraction in both the hydrogels and the organoid, leading to their compaction (Fig. 3f). During maturation, coordinated cell movement and rearrangement are observed, manifesting as a spiral movement within the alveoli (Supplementary Video 8). This observation was made possible due to lentiviral transduction of primary cells, prior to embedding in the hydrogel, with a vector containing the gene encoding the fluorescent protein Venus downstream of the spleen focus-forming virus promoter (SFFV, Addgene plasmid LeGO-V2 #27340 [21]), resulting in stable expression of Venus in the transduced cells.

This fine-tuned methodology has allowed us to observe, in real time, the intricate processes of organoid formation from primary breast epithelial cells. Single cells divide to establish a niche and progeny where one group of cells influences the development of another group of cells through close-range interactions. This nuanced understanding can provide foundational insights into organ development, cellular and molecular mechanisms underlying tissue regeneration, and disease mechanisms.

Hormone responsive model for androgen treatment on human breast tissue

We next explored the potential of this model to investigate the impact of hormones on breast tissue organogenesis. Two key hormones, estrogen and progesterone, are pivotal for breast development. Their roles have been extensively studied [22,23], and a decline in their levels post-menopause is linked to breast tissue atrophy [24,25]. An analogous atrophy is seen in F-M transition patients, wherein individuals undergo long-term androgen hormone therapy [26]. However, due to limited model systems, the functional implications of this atrophy on stem cell function and breast tissue regeneration remain unexplored.

We seeded cells from breast tissue collected from mastectomy surgeries of patients undergoing F-M transition who had been undergoing androgen therapy (n=5). In parallel, we also seeded cells from breast reduction surgeries of post-menopausal patients (n=6) to examine how different hormonal influences on the human breast affected organoid formation. Compared to pre-menopausal patient samples (n=12), cells from post-menopausal patients had a statistically significant 19.7-fold reduction in the rate of organoid formation (0.11 ± 0.05 and 2.12 ± 0.59 (mean ± SEM)) (Fig. 4a). Interestingly, organoid formation from cells of F-M patients also showed a reduced capacity (~2.3 fold) compared to pre-menopausal patients (0.93 ± 0.43 mean ± SEM), although this did not reach statistical significance due to the small sample size. In addition, organoids from F-M samples differed in structure, size, and complexity compared to pre-menopausal organoids. The organoids from F-M samples resembled rudimentary structures classified as acinar, budding acinar, and ductal, rather than the complex, gland-like ductal-lobular structures often observed in pre-menopausal samples (Fig. 4b).

Using luminal (EpCAM) and basal (CD49f) epithelial markers, we compared the epithelial vs. non-epithelial populations among pre-menopausal (n=14), post-menopausal (n=6),

and F-M (n=15) samples to determine whether reduced organoid formation from post-menopausal and F-M breast tissue was due to differences in the proportion or types of epithelial cell types seeded (Fig. 4c, d). Three cell populations were identified: luminal ($EpCAM^{high}$), basal ($EpCAM^{neg/low}/CD49f^{pos}$), and non-epithelial (NE; $EpCAM^{neg}/CD49f^{neg}$). While the percentage of luminal cells did not statistically differ between pre- and post-menopausal samples, the percentage of luminal cells was significantly reduced in F-M samples compared with pre-menopausal samples (Fig. 4c). The percentage of basal and NE cells did not differ between the groups. Notably, in most pre-menopausal and F-M samples, we observed two types of basal cells, categorized as $EpCAM^{neg}$ and $EpCAM^{low}$, as well as two types of luminal cells, identified as $CD49f^{neg}$ and $CD49f^{pos}$ (Fig. 4d). In contrast, post-menopausal samples exhibited reduced cell diversity and showcased a singular basal cell type, $EpCAM^{neg}$, and a single luminal type, $CD49f^{low}$.

Together, these results indicate that post-menopausal involution and androgen-induced mammary tissue atrophy post F-M transition are distinct in terms of cell regeneration capacity and effects on epithelial cell diversity. It's notable that F-M transition samples exhibit a cellular diversity similar to pre-menopausal women, yet these cells have lost their ability to form organoids. This suggests that despite having similar cellular markers, the cells from F-M transition individuals may have undergone functional changes.

We next tested whether treatment with estrogen or progesterone might enhance the decreased regenerative capacity of F-M samples. Hydrogels seeded with cells derived from F-M patients (n=5) were cultured for 21 days in the presence of estrogen (E2), with or without the further addition of progesterone (P). E2 and P treatment did not affect the morphology or rate of

organoid formation (Fig. 4e, f), suggesting that E2+P ex-vivo could not rescue the changes androgen therapy induced on breast cells in vivo. These experiments demonstrate that androgen treatment affects the regenerative capacity of breast epithelial cells, both in quantity and quality, and that the presence of estrogen or progesterone in the culture media cannot readily reverse these effects. In addition, these findings underscore the multifaceted impact of hormonal changes on breast tissue.

Discussion

The inherent ability of cells to organize themselves is a cornerstone of organoid technology. Yet tissue development in vivo does not proceed via spontaneous self-assembly but is driven by directed organogenesis programs. In this study, we have advanced the current paradigm of organoid technology by pioneering a method that promotes directed tissue organogenesis as opposed to spontaneous self-assembly seen in traditional organoid models. This nuanced approach enables the production of organoids that more faithfully replicate in vivo tissues. For the breast, we found that these organoids are indistinguishable from human breast tissue on an anatomical, cellular, and molecular level. This is invaluable for studying cellular processes, interactions, and signaling pathways that derived development, aging, tissue repair, and even cancer. Having a more realistic model which includes both epithelial and stromal cells allows for the study of cancer formation, progression, and stromal-epithelial interactions that are not possible with current 3D models. Having realistic organoid models also enables drug testing in conditions that closely resemble human tissues. This increases the chances that drugs effective in organoid models will also be effective in patients. Moreover, organoids can be grown from individual patients, allowing for personalized medicine approaches where drug responses can be predicted for a particular individual. Finally, using this organoid model and tracking method, it will now be possible with the aid of various molecular and genetic labeling tools, to observe how cells divide, migrate, transdifferentiate, and interact with each other and with the extracellular matrix to form tissues in real time.

In addition to the technological advancement, this new method has also provided several additional insights. First, we observed that breast organoid formation reactivates the latent

developmental program emphasizing induction, patterning, morphogenesis and differentiation. Traditional breast 3D organoid models spontaneously self-assemble in Matrigel or Type I Collagen mimic only rudimentary aspects of development. Cells adhere to specific neighboring cells, establish polarity, form lumen, and create multicellular structures, by leveraging their intrinsic properties [27]. The physical environment of the hydrogels however, combined with the live imagining has allowed for the visualization of epithelial induction and patterning in an unprecedented way. We observed two types of induction both of which were foundational phases of organoid development but exhibited different behaviors. In one type of induction, the static behavior of cells appeared to be primarily geared towards preparation for further growth and differentiation that culminated to the ejection of cells from the static colony. In the second type of induction, the initiation of cell proliferation and migration suggests that the cells are preparing for a phase of rapid growth or expansion. Further studies are needed to understand the cellular, molecular, and environmental basis of these types of induction.

We also observed that ductal branching of organoids occurs through patterning. While the participation of leader cells and group cell movement in branching morphogenesis is well documented, the patterning phenomenon observed here, where cells are entirely detached from the branch, and precedes branching by days, has not been reported. Additional studies are needed to further understand this newly identified process. Insights into breast morphogenesis have also been made in this model. Similar to the spiral cell movements in branched lung organoids, breast organoids also exhibit spiral cell movements [27]. The significance of this remains unknown.

Second, this method facilitates real-time observation of cell lineage plasticity, a process that has not been currently achievable. We observed multi-lineage induction from single adult cells, implying that both epithelium and mesenchyme originate from the same precursor cell.

Indeed, human breast tissue has been shown to contain cells that exhibit extensive plasticity and multi-lineage potential when removed from their native tissue microenvironment [28].

Third, we observed a prominent population of mesenchymal cells by scRNA-seq and functionally playing an active role in tissue architecture, assisting in the organoid structure's integrity and stromal remodeling. Further verification and examination of mesenchymal cell origins in the organoid model is warranted. While we have previously observed, using static microscopy imaging, that some organoids are surrounded by mesenchymal-looking cells (Fig. 3f), their hyper-motility and participation in organoid maturation were only revealed through live imaging. The mesenchymal cells, with their pivotal role in the organoid's structural integrity and stromal remodeling, warrant further exploration in subsequent studies.

Methods

Ethics statement

Primary tissues that would otherwise have been discarded as medical waste following surgery were obtained in compliance with all relevant laws, using protocols approved by the institutional review board at Maine Medical Center and Tufts Medical Center. All tissues were anonymized before transfer and could not be traced to specific patients; for this reason, this research was provided exemption status by the Committee on the Use of Humans as Experimental Subjects at the Massachusetts Institute of Technology, and at Tufts University Health Sciences (IRB# 13521). All patients enrolled in this study signed an informed consent form to agree to participate in this study and for publication of the results.

Tissue processing and 3D culture.

Tissues were partially dissociated with 1.5mg/ml collagenase (10103578001, Millipore Sigma) and 18μg/ml hyaluronidase (H3506, Sigma Aldrich), yielding small epithelial fragments, washed, and cryopreserved in 1 mL aliquots. Tissue fragments were further dissociated to single cells using 0.25% trypsin (25200056, Thermo Fisher Scientific) and 5 U/ml dispase II (4942078001, Roche). Hydrogels were seeded at a concentration of 500 cells per 200 μL gel (2.5 cells/μL). For hydrogel fabrication and seeding, cells were resuspended in 1.7 mg/ml collagen I (08-115, Millipore Sigma), 10 μg/ml hyaluronic acid (385908, Millipore Sigma) 40 μg/ml laminin (23017-015, Gibco), and 20 μg/ml fibronectin (F1056, Sigma Aldrich), pH 7.3. Gels were deposited in 4-well chamber slides (354104, Falcon) and incubated 1 hour at 37 °C for polymerization before adding MEGM medium [10]. Hydrogels were cultured floating in serum-free

mammary epithelial growth media (MEGM) in 4-well chamber slides. MEGM consisted of basal medium (M171500, Thermo Fisher Scientific) supplemented with 52μg/ml bovine pituitary extract (13028014, Thermo Fisher Scientific), 10ng/ml hEGF (E9644, Sigma Aldrich), 5μg/ml insulin (I9278, Sigma Aldrich), 500ng/ml hydrocortisone (H0888, Sigma Aldrich), 1% v/v GlutaMAX (35050061, Thermo Fisher Scientific), and 1% v/v penicillin-streptomycin antibiotics (15140122, Thermo Fisher Scientific).

Immunofluorescent Staining of Hydrogels

Hydrogels were fixed with 4% paraformaldehyde (15710-S, Electron Microscopy Sciences) at room temperature for 30 minutes and washed in PBST, comprised of 1X PBS (46-013-CM, Corning) and 0.05% Tween 20 (P7949, Millipore Sigma). Samples were then permeabilized in 0.1% TritonX-100 (X100, Sigma Aldrich) in PBST and incubated with blocking buffer comprised of PBST with 3% BSA (BSA-50, Rockland Immunochemicals) and 10% goat serum (G9023, Millipore Sigma) for 2 hours at room temperature. Hydrogels were then stained with the appropriate primary antibody in blocking buffer at 4°C overnight. Samples were washed with PBST and incubated with secondary antibody for 2 hours at room temperature, and DAPI for 30 minutes at room temperature. Primary antibodies used in this study were: E-cadherin (ab1416, Abcam, Clone HECD-1, 1:100), CK14 (RB-9020, Thermo Fisher, 1:300). Secondary antibodies used in this study were: goat-anti-mouse-AF555 (A21424, Life Technologies, 1:1000), goat-anti-rabbit-AF488 (A11008, Life Technologies, 1:1000). Dyes and probes used for immunofluorescence: Phalloidin-AF647 (A22287, Life Technologies, 1:250 of 400x stock), DAPI (D1306, Life Technologies, 5μg/ml).

FFPE Patient Tissue Staining

Patient tissue was fixed in 10% buffered formalin and paraffin-embedded in tissue blocks which were serially sectioned. Slides were baked at 55°C for 45 min, then rehydrated by sequential incubation in Xylene, 100% ethanol, 95% ethanol, 70% ethanol, and 50% ethanol for 3 minutes each, then 10 minutes in PBS. Antigen retrieval was done in sodium citrate buffer in a steamer for 20 minutes. Slides were washed in TBS-T comprised of 1X TBS (Trizma base, T4661, Millipore Sigma; NaCl, 71376, Millipore Sigma) and 0.25% TritonX-100 and then in blocking buffer, comprised of TBS-T with 10% goat serum and 1% BSA, for 2 hours at room temperature. Slides were stained with appropriate primary antibody in blocking buffer at 4°C overnight. Samples were washed with TBS-T and incubated with secondary antibody for 2 hours at room temperature, and DAPI for 30 minutes at room temperature. Slides were washed in tap water and covered with mounting medium and glass coverslips. Primary antibodies used in this study were: E-cadherin (610182, BD Biosciences, Clone 36, 1:50), CK14 (RB-9020, Thermo Fisher, 1:50), Secondary antibodies used in this study were: goat-anti-mouse-AF555 (A21424, Life Technologies, 1:1000), goat-anti-rabbit-AF488 (A11008, Life Technologies, 1:1000). Dyes and probes used for immunofluorescence: DAPI (D1306, Life Technologies, 5μg/ml).

Live imaging

Primary single cells, isolated as described above, were incubated with the cell tracking dye Cytopainter Green (ab138891, Abcam, 1:1000) for 30 minutes and then were washed and seeded at a concentration of 100 cells per 20 μL hydrogel. For gel fabrication, 20 μL hydrogel drops were deposited onto the center wells of a 96-well plate (3603, Corning). Gels were allowed to incubate for one hour at 37°C until fully polymerized. 80μL of MEGM was then added to each

well and gels were gently lifted off the well surface with a pipette tip. Cultures were immediately placed in a pre-warmed incubator chamber (Okolab Inc) enclosed over a Nikon Eclipse Ti2-AX confocal microscope (Nikon). Images of selected points were collected starting immediately after the addition of media, and every 30-45 minutes after, in both brightfield and with A488 laser at 4x magnification and 2.5x zoom across nine z-positions. 20-40 μL media was added to the culture twice a week. Cultures were live imaged for 18-21 days. Analysis and production of videos across locations and timepoints was performed using NIS-Elements (Nikon) and Premiere Pro (Adobe) software.

scRNA-seq analysis

We analyzed previously published scRNA-seq data from orgnaoids[11] and healthy primary breast tissue[12]. scRNA-seq data was analyzed using Seurat v3[29] for data integration, normalization, and feature selection. Briefly, raw data was loaded and integrated into one Seurat object using the merge function. Filtering removed cells with < 200 or >2500 genes and with mitochondrial content greater than 7.5%. Genes detected in less than 3 cells were dropped from analysis. The data was then normalized by multiplying transcripts by a factor of 10,000 and then log-transforming the data. Variable features used for analysis were identified by using the FindVariableFeatures function, with a low cutoff of 0.0125 and a high cutoff of 5 for dispersion and a low cutoff of 0.1 and a high cutoff of 0.8 for average expression. The data was integrated by the FindIntegrationAnchors and IntegrateData functions, which identify the anchors to integrate the two datasets, and then integrates them together. Cells were then clustered using K-nearest neighbor (KNN) graphs and the Louvain algorithm using the first 15 dimensions from principal component analysis. Clustered cells were visualized by tSNE embedding using the

default settings in Seurat. Clusters were called using the FindClusters function with a resolution of 0.4, and 14 distinct cell clusters were identified. To identify differentially expressed genes between cell clusters, we utilized the FindAllMarkers function to identify features detected in >10% of a cell cluster compared to all other cells. Pathway analysis to identify enriched biological pathways associated with differentially expressed genes was done using established databases, such as PanglaoDB [30]. The top 15 differentially expressed markers were used to determine gene expression location.

Hormone treatment

200 μL hydrogels were seeded with single primary cells from F-M patients (n=5) and post-menopausal patients (n=6), at a concentration of 1500 cells per hydrogel. Hydrogels were deposited and cultured floating in 4-well chamber slides. Media consisted of phenol red-free MEGM (CC-3153, Lonza) supplemented the same as MEGM media (listed under Tissue Processing and 3D Culture). All hormone supplements were dissolved in 0.5% DMSO. For hormone treatment experiments, media was supplemented with either 0.5% DMSO (317275, Millipore Sigma), 1nM 17β-estradiol (E2; E2758, Sigma), or 1 nM 17β-estradiol + 1 nM progesterone (P4; P0130, Sigma). Hydrogels were cultured for each F-M patient sample (n=8) under each treatment condition, and for each post-menopausal patient sample (n=4). Hydrogels were cultured in hormone treatment media for 21 days with media changes occurring every two days. Organoid number and morphology were analyzed on day 21 using an Eclipse Ti-U microscope (Nikon).

Flow Cytometry

Single cells dissociated from patient tissues as described above were washed with PBS with 2% FBS and stained with antibodies at 4°C for 60 minutes. Cells were then washed and resuspended in PBS with 2% FBS for flow cytometry. All data acquisition was done using an LSR II (BD Biosciences) and analyzed using FlowJo software (TreeStar). Antibodies used for flow cytometry: CD49f-FITC (555735, BD Biosciences, 1:20), EpCAM-APC (347200, BD Biosciences, 1:20).

Acknowledgments

This research was supported by the following: NIGMS (7R01GM124491, CK), DOD-BCRP (W81XWH2010018, GR), Breast Cancer Research Foundation (CK) and FTC Breast Cancer Foundation (CK)

Author Contributions

GR, NCT, CJT, MEP and CK conceived the project and designed experiments. GR, NCT, CJT, MEP and KM performed experiments. GR, NCT, CJT, MEP and CK analyzed results GR, NCT, CJT, MEP and CK wrote the manuscript with contributions, editorial review, and approval from all authors.

Competing Interests

GR consults for Turtle Tree Inc.

CK is co-founder and consultant of Naveris Inc.

Figure Legends

Fig. 1: Regenerative and biomimetic capacity of breast organoids

a, List of tissue donor patients with age and body mass index (BMI). **b**, Representative bright field images of organoid morphology types. Scale bar = 100 µm. **c,** Proportion of organoid morphologies. Mean ± STD. **d,** Rate of organoid formation per 100 cells from 12 patient samples (n=4 repeats per sample). Mean ± SEM. **e**, Rate of organoid formation across patient samples. Median ± 95% CI. **f**, Rate of primary and secondary organoid formation of 5 patient samples (n=4 repeats per sample). Mean ± SEM. **g**, Rate of secondary organoid formation across 5 patient samples. Median ± 95% CI. **h**, Whole-gel images of bright-field (left panels) and immunofluorescence staining for F-actin (phalloidin, magenta) with DAPI (blue, middle panels), and E-cadherin (red) with CK14 (green, right panels). Scale bars = 1mm. **i**, Side-by-side comparison of organoid (right) and patient tissue (left) immunostaining for CK14 (green), E-cadherin (red) and DAPI (blue). Scale bars = 100 µm.

Fig. 2: scRNA-seq analysis of breast tissue and next-generation organoids

a, Side-by-side comparison of scRNA-seq clustering of cells derived from healthy human breast tissue and breast tissue organoids. **b-j**, Expression patterns highlighting luminal markers KRT8, KRT18, KRT19, CD24, ESR1, PGR, ELF5, SFRP1, and KIT. **k-m,** Expression patterns highlighting basal markers KRT5, KRT14, and KRT17. **n-r**, Expression patterns highlighting stromal fibroblast markers PDGFRB1, COL1A2, COL6A3, THY1, and ZEB1.

Fig. 3: Live Imaging of Cellular Dynamics in Breast Organoid Development

a, Schematic representation of the high-throughput confocal live imaging setup for observing human breast organogenesis and maturation in the organoid model. The diagram details the experimental design and methodology. **b**, Panel of selected frames from Supplementary Video 1, demonstrating the four phases of organoid development, with Type I induction. Scale bar = 100 μm. **c,** Schematic representation and timeline of the 4 phases of organoid development, including Type I and Type II induction. **d**, Panel of selected frames from Supplementary Video 8, showing type II induction culminating with cell (red arrowheads) detaching and moving away, branch subsequently grows in the direction of the preceding cell. Scale bar = 100 μm. **e**, Immunostaining of organoids, at different stages of development, for CK14 (green), E-cadherin (red) and DAPI (blue). Scale bars = 50 μm. **f**, Mature organoid producing the classic morphology of a terminal ductal-lobular unit embedded within compacted mesenchyme. Scale bar = 100 μm.

Fig. 4: Effects of Androgen Treatment on Human Breast Tissue Regeneration and Morphology in a Hormone Responsive Model.

a, Comparison of the rate of organoid formation per 100 cells between breast tissues from pre-menopausal, post-menopausal, and F-M transition patients. Mean ± SEM. **b,** Morphological classification of the developing structures: acinar, budding acinar, and ductal categories in the presence of hormone treatments. Scale bar = 100 μm. **c,** Percent distribution of epithelial (luminal and basal) and non-epithelial (NE) cell populations among pre-menopausal, post-menopausal, and F-M patient samples. (* p=0.0461, one way ANOVA with Sidak's multiple comparisons test). **d,** Flow cytometry analysis for luminal (EpCAM) and basal (CD49f) epithelial markers. Gating of basal, luminal and non-epithelial (NE) populations in pre-menopausal, post-menopausal, and F-M samples. **e,** Percent distribution of organoid morphologies that developed in the presence of hormone treatments. Mean ± SEM. **f,** Organoid

number in hydrogels seeded with F-M patient-derived cells after treatment with estrogen (E), with or without progesterone (P), compared to a DMSO vehicle control. Mean ± SEM.

References

1 Rosenbluth, J. M. *et al.* Organoid cultures from normal and cancer-prone human breast tissues preserve complex epithelial lineages. *Nature Communications* **11**, 1711 (2020). https://doi.org:10.1038/s41467-020-15548-7

2 Florian, S., Iwamoto, Y., Coughlin, M., Weissleder, R. & Mitchison, T. J. A human organoid system that self-organizes to recapitulate growth and differentiation of a benign mammary tumor. *Proceedings of the National Academy of Sciences* **116**, 11444-11453 (2019). https://doi.org:doi:10.1073/pnas.1702372116

3 Sumbal, J., Budkova, Z., Traustadóttir, G. & Koledova, Z. Mammary Organoids and 3D Cell Cultures: Old Dogs with New Tricks. *J Mammary Gland Biol Neoplasia* **25**, 273-288 (2020). https://doi.org:10.1007/s10911-020-09468-x

4 Barcellos-Hoff, M. H., Aggeler, J., Ram, T. G. & Bissell, M. J. Functional differentiation and alveolar morphogenesis of primary mammary cultures on reconstituted basement membrane. *Development* **105**, 223-235 (1989). https://doi.org:10.1242/dev.105.2.223

5 Li, M. L., Aggeler, J., Farson, D. A., Hatier, C., Hassell, J. & Bissell, M. J. Influence of a reconstituted basement membrane and its components on casein gene expression and secretion in mouse mammary epithelial cells. *Proc Natl Acad Sci U S A* **84**, 136-140 (1987). https://doi.org:10.1073/pnas.84.1.136

6 Nguyen-Ngoc, K.-V., Shamir, E. R., Huebner, R. J., Beck, J. N., Cheung, K. J. & Ewald, A. J. in *Tissue Morphogenesis: Methods and Protocols* (ed Celeste M. Nelson) 135-162 (Springer New York, 2015).

7 Sumbal, J., Chiche, A., Charifou, E., Koledova, Z. & Li, H. Primary Mammary Organoid Model of Lactation and Involution. *Frontiers in Cell and Developmental Biology* **8** (2020). https://doi.org:10.3389/fcell.2020.00068

8 Ciccone, M. F., Trousdell, M. C. & dos Santos, C. O. Characterization of Organoid Cultures to Study the Effects of Pregnancy Hormones on the Epigenome and Transcriptional Output of Mammary Epithelial Cells. *Journal of Mammary Gland Biology and Neoplasia* **25**, 351-366 (2020). https://doi.org:10.1007/s10911-020-09465-0

9 Ewald, A. J., Brenot, A., Duong, M., Chan, B. S. & Werb, Z. Collective epithelial migration and cell rearrangements drive mammary branching morphogenesis. *Dev Cell* **14**, 570-581 (2008). https://doi.org:10.1016/j.devcel.2008.03.003

10 Sokol, E. S., Miller, D. H., Breggia, A., Spencer, K. C., Arendt, L. M. & Gupta, P. B. Growth of human breast tissues from patient cells in 3D hydrogel scaffolds. *Breast Cancer Res* **18**, 19 (2016). https://doi.org:10.1186/s13058-016-0677-5

11 Rauner, G. *et al.* Breast tissue regeneration is driven by cell-matrix interactions coordinating multi-lineage stem cell differentiation through DDR1. *Nat Commun* **12**, 7116 (2021). https://doi.org:10.1038/s41467-021-27401-6

12 Gray, G. K. *et al.* A human breast atlas integrating single-cell proteomics and transcriptomics. *Dev Cell* **57**, 1400-1420 e1407 (2022). https://doi.org:10.1016/j.devcel.2022.05.003

13 Cunha, G. R. & Hom, Y. K. Role of mesenchymal-epithelial interactions in mammary gland development. *J Mammary Gland Biol Neoplasia* **1**, 21-35 (1996). https://doi.org:10.1007/bf02096300
14 Cowin, P. & Wysolmerski, J. Molecular mechanisms guiding embryonic mammary gland development. *Cold Spring Harb Perspect Biol* **2**, a003251 (2010). https://doi.org:10.1101/cshperspect.a003251
15 Varner, V. D. & Nelson, C. M. Cellular and physical mechanisms of branching morphogenesis. *Development* **141**, 2750-2759 (2014). https://doi.org:10.1242/dev.104794
16 Wang, S., Sekiguchi, R., Daley, W. P. & Yamada, K. M. Patterned cell and matrix dynamics in branching morphogenesis. *Journal of Cell Biology* **216**, 559-570 (2017). https://doi.org:10.1083/jcb.201610048
17 Benitah, S. A. & Frye, M. Stem cells in ectodermal development. *J Mol Med (Berl)* **90**, 783-790 (2012). https://doi.org:10.1007/s00109-012-0908-x
18 Tadeu, A. M. *et al.* Transcriptional profiling of ectoderm specification to keratinocyte fate in human embryonic stem cells. *PLoS One* **10**, e0122493 (2015). https://doi.org:10.1371/journal.pone.0122493
19 Byrne, C., Tainsky, M. & Fuchs, E. Programming gene expression in developing epidermis. *Development* **120**, 2369-2383 (1994). https://doi.org:10.1242/dev.120.9.2369
20 Makarem, M., Spike, B. T., Dravis, C., Kannan, N., Wahl, G. M. & Eaves, C. J. Stem cells and the developing mammary gland. *J Mammary Gland Biol Neoplasia* **18**, 209-219 (2013). https://doi.org:10.1007/s10911-013-9284-6
21 Weber, K., Bartsch, U., Stocking, C. & Fehse, B. A multicolor panel of novel lentiviral "gene ontology" (LeGO) vectors for functional gene analysis. *Mol Ther* **16**, 698-706 (2008). https://doi.org:10.1038/mt.2008.6
22 Arendt, L. M. & Kuperwasser, C. Form and function: how estrogen and progesterone regulate the mammary epithelial hierarchy. *J Mammary Gland Biol Neoplasia* **20**, 9-25 (2015). https://doi.org:10.1007/s10911-015-9337-0
23 Shyamala, G. Roles of estrogen and progesterone in normal mammary gland development insights from progesterone receptor null mutant mice and in situ localization of receptor. *Trends Endocrinol Metab* **8**, 34-39 (1997). https://doi.org:10.1016/s1043-2760(96)00207-x
24 Lin, J. *et al.* Changes in the mammary gland during aging and its links with breast diseases. *Acta Biochim Biophys Sin (Shanghai)* **55**, 1001-1019 (2023). https://doi.org:10.3724/abbs.2023073
25 Walker, R. A. & Martin, C. V. The aged breast. *J Pathol* **211**, 232-240 (2007). https://doi.org:10.1002/path.2079
26 Smith, K. P., Madison, C. M. & Milne, N. M. Gonadal Suppressive and Cross-Sex Hormone Therapy for Gender Dysphoria in Adolescents and Adults. *Pharmacotherapy: The Journal of Human Pharmacology and Drug Therapy* **34**, 1282-1297 (2014). https://doi.org:https://doi.org/10.1002/phar.1487

27 Srivastava, V., Huycke, T. R., Phong, K. T. & Gartner, Z. J. Organoid models for mammary gland dynamics and breast cancer. *Current Opinion in Cell Biology* **66**, 51-58 (2020). https://doi.org:https://doi.org/10.1016/j.ceb.2020.05.003

28 Van Keymeulen, A. *et al.* Distinct stem cells contribute to mammary gland development and maintenance. *Nature* **479**, 189-193 (2011). https://doi.org:10.1038/nature10573

29 Stuart, T. *et al.* Comprehensive Integration of Single-Cell Data. *Cell* **177**, 1888-1902 e1821 (2019). https://doi.org:10.1016/j.cell.2019.05.031

30 Franzen, O., Gan, L. M. & Bjorkegren, J. L. M. PanglaoDB: a web server for exploration of mouse and human single-cell RNA sequencing data. *Database (Oxford)* **2019** (2019). https://doi.org:10.1093/database/baz046

Figure 1

a

Patient ID	Age	BMI
P3	18	20.83
P4	26	21.07
P5	33	26.74
P6	25	27.95
P7	18	28.43
P8	26	21.83
P9	18	23.69
P10	29	28.55
P11	20	28.06
P12	22	23.92
P13	29	20.67
P14	27	27.04

b

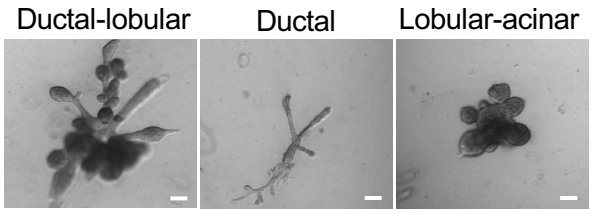

c

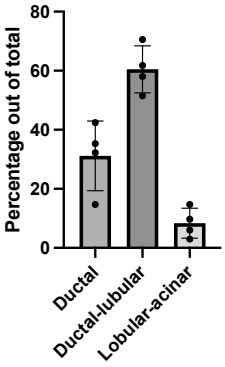

d

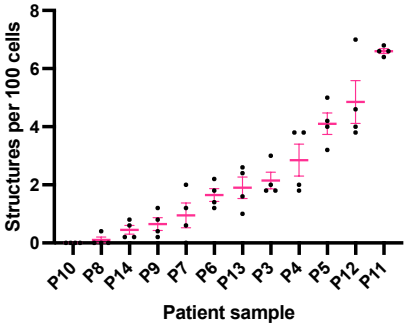

e

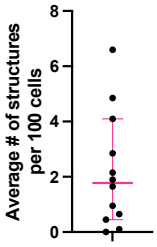

f

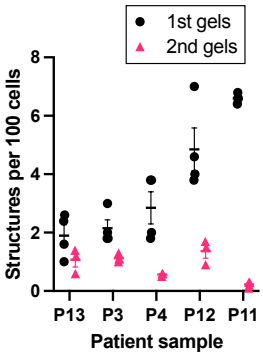

g

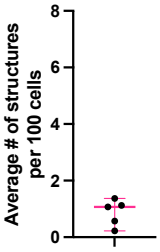

h

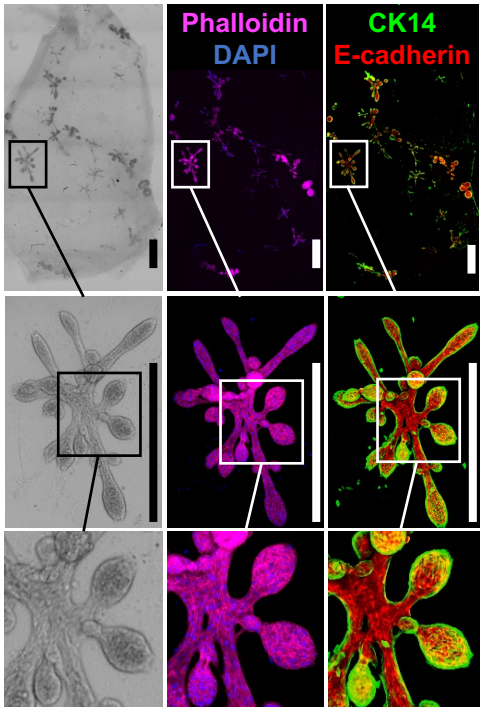

i

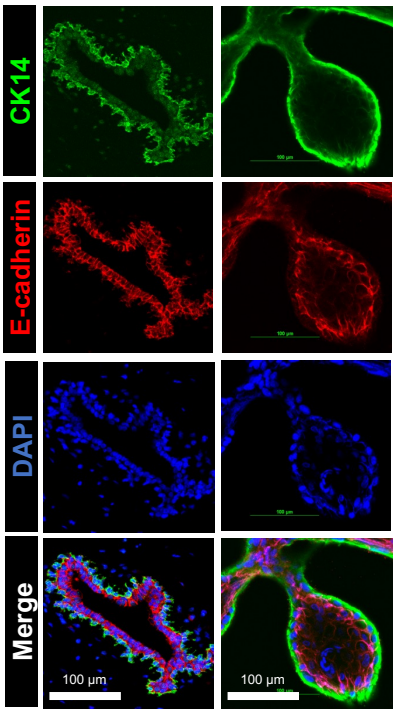

Figure 2

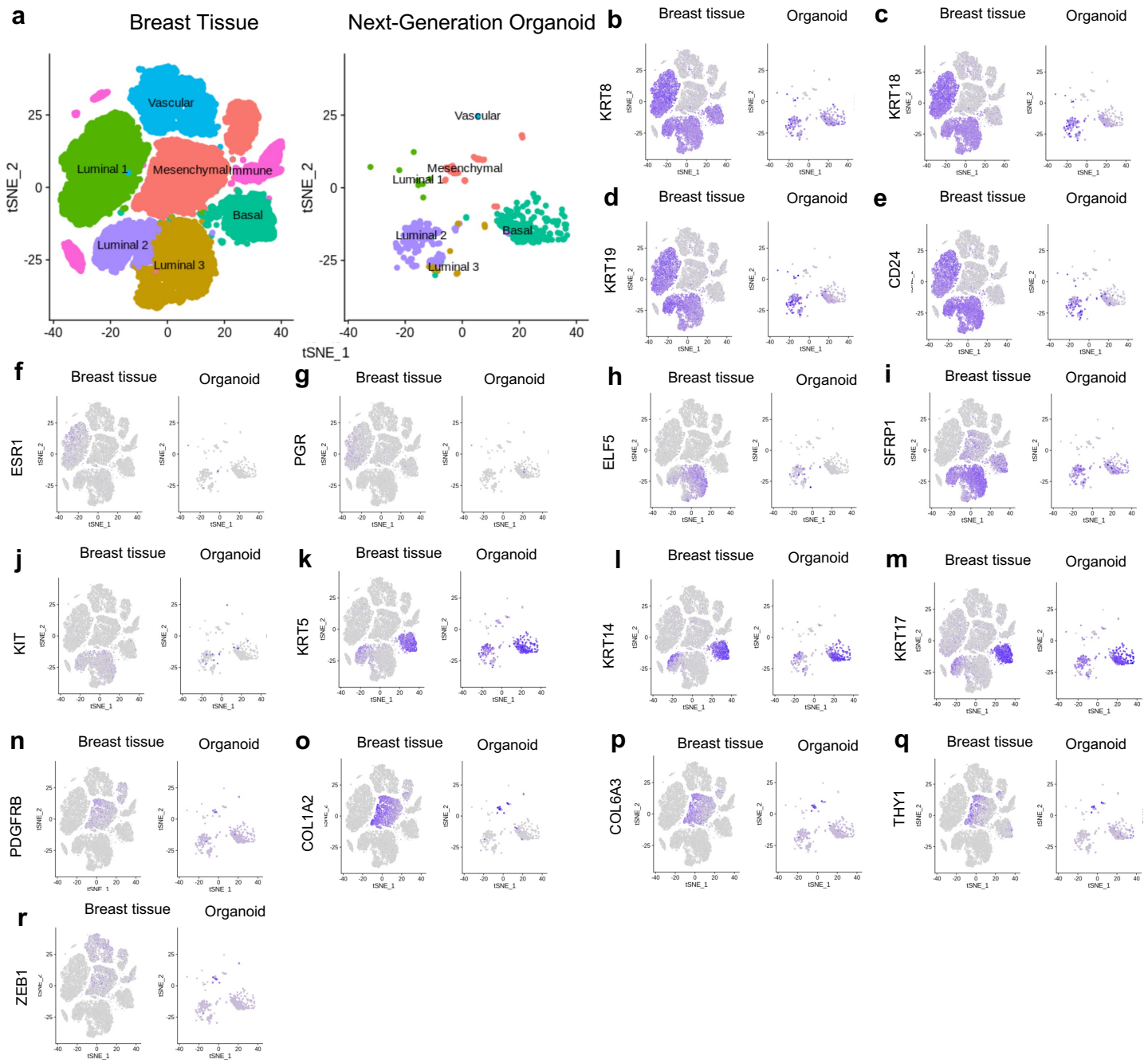
a
Breast Tissue
Next-Generation Organoid
Vascular
Luminal 1
Mesenchymal
Immune
Basal
Luminal 2
Luminal 3
tSNE_1
tSNE_2
b
c
d
e
f
g
h
i
j
k
l
m
n
o
p
q
r
Breast tissue
Organoid
KRT8
KRT18
KRT19
CD24
ESR1
PGR
ELF5
SFRP1
KIT
KRT5
KRT14
KRT17
PDGFRB
COL1A2
COL6A3
THY1
ZEB1

Figure 3

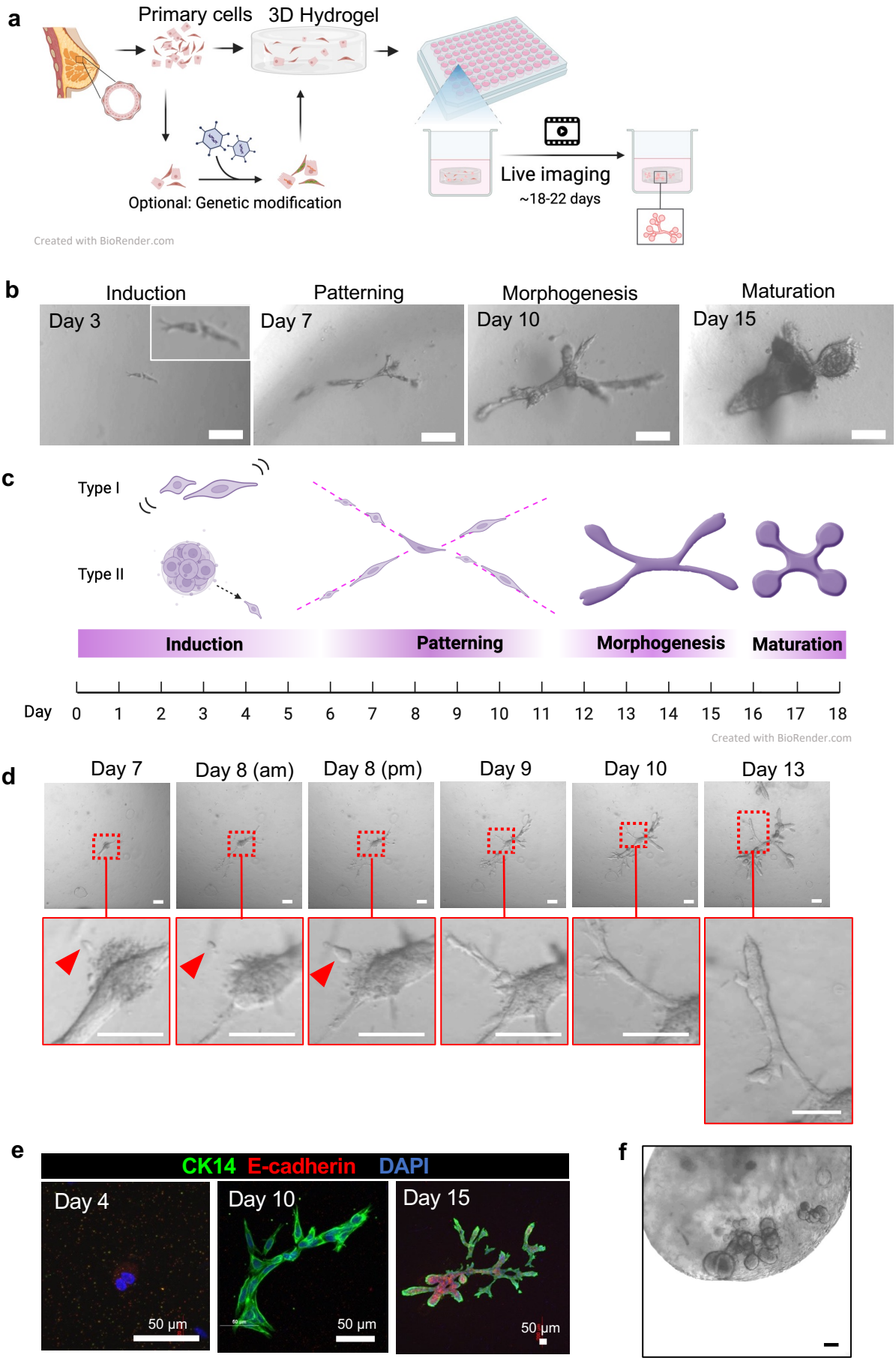
a
Primary cells
3D Hydrogel
Optional: Genetic modification
Live imaging
~18-22 days
Created with BioRender.com
b
Induction
Patterning
Morphogenesis
Maturation
Day 3
Day 7
Day 10
Day 15
c
Type I
Type II
Induction
Patterning
Morphogenesis
Maturation
Day 0 1 2 3 4 5 6 7 8 9 10 11 12 13 14 15 16 17 18
Created with BioRender.com
d
Day 7
Day 8 (am)
Day 8 (pm)
Day 9
Day 10
Day 13
e
CK14 E-cadherin DAPI
Day 4
Day 10
Day 15
50 µm
50 µm
50 µm
f

Figure 4

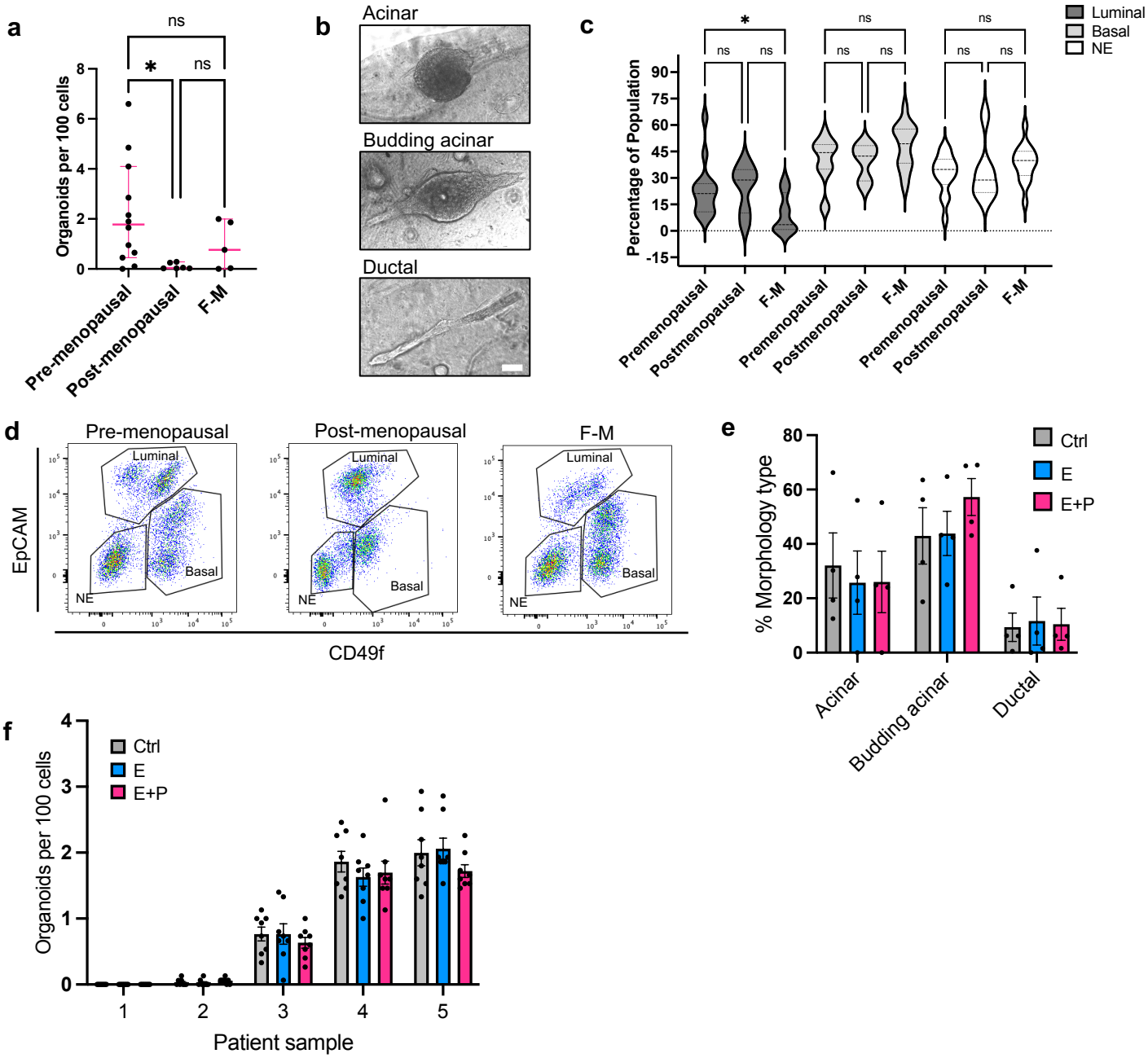
a
ns
*
ns
Organoids per 100 cells
Pre-menopausal
Post-menopausal
F-M
b
Acinar
Budding acinar
Ductal
c
Luminal
Basal
NE
Percentage of Population
Premenopausal
Postmenopausal
F-M
d
Pre-menopausal
Post-menopausal
F-M
Luminal
Basal
NE
EpCAM
CD49f
e
% Morphology type
Ctrl
E
E+P
Acinar
Budding acinar
Ductal
f
Organoids per 100 cells
Patient sample